

Dedicated 3D photoacoustic breast imaging

Robert A. Kruger^{a)}

OptoSonics, Inc., 108 Straight Road, Oriental, North Carolina 28571

Cherie M. Kuzmiak

*Department of Radiology, University of North Carolina Lineberger Comprehensive Cancer Center,
University of North Carolina at Chapel Hill, CB# 5120, Manning Drive, Chapel Hill,
North Carolina 27599-7510*

Richard B. Lam, Daniel R. Reinecke, and Stephen P. Del Rio

OptoSonics, Inc., 108 Straight Road, Oriental, North Carolina 28571

Doreen Steed

TraCS Institute, University of North Carolina at Chapel Hill, Chapel Hill, North Carolina 27599-7510

(Received 23 July 2013; revised 4 September 2013; accepted for publication 20 September 2013;
published 10 October 2013)

Purpose: To report the design and imaging methodology of a photoacoustic scanner dedicated to imaging hemoglobin distribution throughout a human breast.

Methods: The authors developed a dedicated breast photoacoustic mammography (PAM) system using a spherical detector aperture based on our previous photoacoustic tomography scanner. The system uses 512 detectors with rectilinear scanning. The scan shape is a spiral pattern whose radius varies from 24 to 96 mm, thereby allowing a field of view that accommodates a wide range of breast sizes. The authors measured the contrast-to-noise ratio (CNR) using a target comprised of 1-mm dots printed on clear plastic. Each dot absorption coefficient was approximately the same as a 1-mm thickness of whole blood at 756 nm, the output wavelength of the Alexandrite laser used by this imaging system. The target was immersed in varying depths of an 8% solution of stock Liposyn II-20%, which mimics the attenuation of breast tissue (1.1 cm^{-1}). The spatial resolution was measured using a 6 μm -diameter carbon fiber embedded in agar. The breasts of four healthy female volunteers, spanning a range of breast size from a brassiere C cup to a DD cup, were imaged using a 96-mm spiral protocol.

Results: The CNR target was clearly visualized to a depth of 53 mm. Spatial resolution, which was estimated from the full width at half-maximum of a profile across the PAM image of a carbon fiber, was 0.42 mm. In the four human volunteers, the vasculature was well visualized throughout the breast tissue, including to the chest wall.

Conclusions: CNR, lateral field-of-view and penetration depth of our dedicated PAM scanning system is sufficient to image breasts as large as 1335 mL, which should accommodate up to 90% of the women in the United States. © 2013 American Association of Physicists in Medicine. [<http://dx.doi.org/10.1118/1.4824317>]

Key words: photoacoustic, ultrasound tomography, breast, mammography, cancer

1. INTRODUCTION

Mammography is the current gold standard for screening asymptomatic women for breast cancer and has been proven to decrease mortality.^{1–3} However, this technology has limitations. In women with dense breasts, mammography has not been proven as sensitive as in the population of women with nondense breasts. In reaction to this problem, researchers are exploring optical imaging of the breast with lasers as a way to eliminate the lesion obscurity resulting from overlapping breast tissue prevalent in women with dense breasts.⁴

In optical imaging of the breast, hemoglobin is the primary component that is evaluated.

Hemoglobin is a strong optical absorber in the near infrared, and its presence in breast masses correlates strongly with angiogenesis and elevated micro-vessel density, which are consistent biomarkers of malignancy.⁵ It has been demon-

strated that when breast cancers reach approximately 1–2 mm (10^6 cells), they are no longer adequately nourished by diffusion, and hypoxia ensues.⁶ Hypoxia induces expression of cytokines like vascular endothelial growth factor (VEGF), leading to the creation of tumor vessels that are characterized by their disorganized structure and leaky capillaries.⁷ Average levels of hemoglobin are reportedly higher in malignant masses relative to “normal” breast tissues.⁸

The absorption coefficient of hemoglobin in whole blood (150 gm/L) is $\sim 0.62 \text{ cm}^{-1}$ at 756 nm,⁹ whereas hemoglobin-free breast tissue parenchyma has a reported absorption coefficient of only $0.04\text{--}0.05 \text{ cm}^{-1}$ at the same wavelength, and the effective scattering coefficient of all breast tissue is between 8 and 12 cm^{-1} .^{10,11} Of note, the resulting effective optical attenuation coefficient for an average breast is therefore $\sim 1.0\text{--}1.3 \text{ cm}^{-1}$, which is only slightly greater than that reported at mammographic x-ray energies ($0.5\text{--}0.8 \text{ cm}^{-1}$),¹² yet

the differential contrast between hemoglobin-rich (tumors, blood vessels) and hemoglobin-deprived (fat, glandular) tissue is significantly greater than the differential contrast between tumor and surrounding breast tissue at x-ray energies.

A laser-based optoacoustic imaging system (LOIS) for detecting breast cancer was proposed over a decade ago by Oraevsky *et al.*¹³ Spatial resolution within the imaging plane is reported to be 0.5 mm, but cross-plane spatial resolution is relatively poor. Another common approach to photoacoustic imaging is to incorporate a pulsed light source into a conventional medical ultrasound probe, e.g., the OPUS (optoacoustic plus ultrasound) system developed by Haisch *et al.*¹⁴ Dynamic acquisition is possible, too, albeit over a single imaging plane. The Twente Photoacoustic Mammoscope, introduced by Manohar *et al.* in 2004, produces 3D images over a 90-mm field of view.¹⁵ Scan time is reported to be 30 min and spatial resolution is 2.3–3.9 mm.

Our specially designed, dedicated 3D Photoacoustic Mammography system uses a low-power, FDA-approved infrared laser and standard medical ultrasound detectors in a unique configuration to image the breast while the patient is prone on a cushioned table.

2. METHODS

The design of our dedicated photoacoustic mammography (PAM) scanning system is derived from our previous work. We demonstrated that hemoglobin could be imaged to a depth of 40 mm in the breast over a 64-mm-wide field of view with submillimeter spatial resolution using infrared light.¹⁶ The PAM scanner, pictured in Fig. 1, consists of an exam table (T) upon which a patient lies prone, placing one breast in a spherically shaped cup (C) thermoformed from a 0.020" thick sheet of polyethylene terephthalate (PETG). This cup was optically clear and displayed >70% acoustic transmission over $\pm 40^\circ$ at 2 MHz. A small amount of clean water is placed in the breast cup of the scanner along with the breast prior to



FIG. 1. Photograph of PAM scanner showing the exam table (T) and the breast positioning cup (C), below which is located the hemispherical detector array.

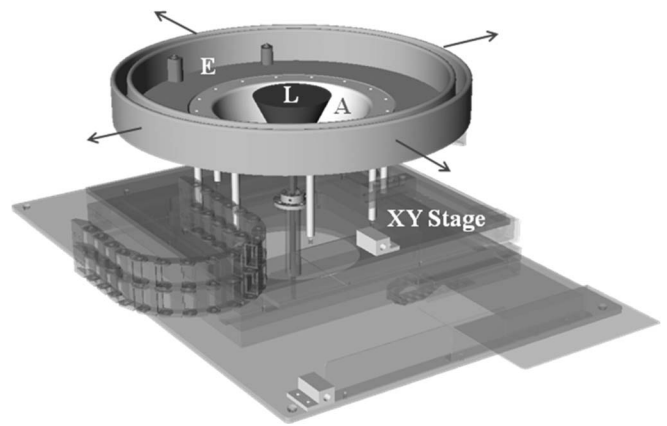


FIG. 2. Drawing showing the hemispherical array (A) mounted on a two-axis translational stage (XY). The hemispherical array and an extension (E) are filled with degassed RO water. Laser light is fed from the bottom of the array via an articulating arm (not shown) through a negative lens that diverges the laser light (L) to a diameter of ~60 mm at the breast surface.

imaging to provide acoustic coupling between the breast and the breast cup.

Figure 2 shows the hemispherical detector array (A), which lies beneath the cup of the scanner, affixed to a two-axis translational stage (XY) whose position is controlled by a pair of computer-controlled, synchronous motors. The water-filled detector array is comprised of a hemispherical shell (radius = 127 mm), machined from ABS plastic, in which are embedded 512 discrete medical ultrasound transducer elements. Each transducer has a flat active area with a 3-mm diameter. The center frequency of the 1–3 piezo-composite transducers is 2 MHz with a 70% bandwidth.

The detector array and a plastic extension (E) to the array were filled with reverse osmosis water to provide acoustic coupling between the breast cup of the scanner and the 512 transducers. A 7-mm-diameter, pulsed Alexandrite laser beam ($\lambda = 756$ nm, 75 ns @ 300 mJ/pulse) was fed through an articulating arm that directed the laser beam (L) upward along the vertical axis of the transducer array as the array was scanned. A -12 mm diverging lens, placed at the base of the array, spread the light in a conical fashion to a diameter of ~60 mm at the surface of the scanner breast cup. The peak light fluence was measured as ~ 10 mJ/cm² at the center of the beam, which is less than half of the maximum permissible exposure (MPE) recommended by the American National Standards Institute.¹⁷

A cutaway of the PAM scanner, which shows the geometric relationships among the detector array, array extension, imaging table, and breast cup, is illustrated in Fig. 3. The array extension allows the detector array to be scanned laterally across the breast surface and still maintain water coupling to the breast. The maximum imaging volume (1335 mL) is defined by the radius of curvature of the breast cup (184 mm), the width of the aperture through which the breast is placed (240 mm), and the maximum penetration depth for which hemoglobin can be visualized. This maximum imaging volume is denoted by the hatching in Fig. 3.

The detector array was scanned continuously in a spiral pattern within a plane, whose normal lay parallel to the

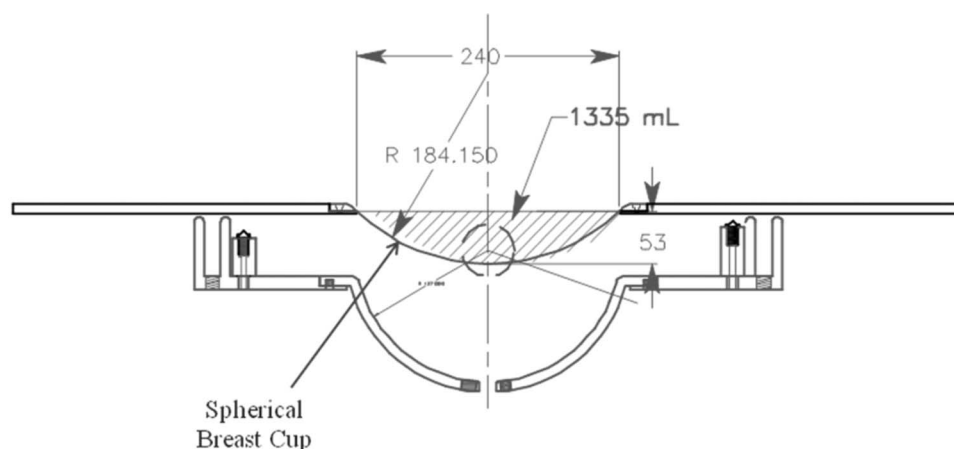


FIG. 3. Cut-away view of imaging geometry showing the relationships among the tabletop, breast positioner (spherical cup of .020" thick PETG), and the detector array.

rotational axis of the array, as the laser beam was pulsed at 10 Hz. The spiral patterns we chose were such that the photoacoustic data were acquired at equidistant locations within a plane, their spacing being the same no matter the size of the spiral. Thus, larger spirals required more pulses and longer image-acquisition times than smaller spirals. Examples of two spiral patterns used for this work are illustrated in Fig. 4. The smallest spiral had a maximum radius of 24 mm and consisted of 120 discrete locations; the largest spiral had a radius of 96 mm and consisted of 1920 discrete locations.

Data from each of the 512 transducers were digitized in parallel after 50 dB of amplification to 12 bits at 20 MHz for a total of 2048 samples following each laser pulse. Data were not integrated. Total data acquisition time was anywhere from 12 s for the smallest spiral to 3.2 min for the largest spiral. The lateral field of view (FOV) varied from 80 mm

to 240 mm diameter, depending on the exact spiral pattern chosen.

Three-dimensional PAM images were reconstructed using a filtered-backprojection algorithm that has been described previously.^{16,18} We first measured the PA response to a "point" absorber fabricated from a small spot of ink placed on the tip of a clear, thin polyethylene thread, which was then used to calculate a ramp filter function and simultaneously deconvolve the impulse response of our transducers. After filtering, we backprojected our data over spherical surfaces, the radii of which were determined from the measured speed of sound in the water coupling and a second, assumed speed of sound within the breast (or phantom). We assumed that everything above the breast cup of the scanner was homogeneous phantom or breast tissue, and everything beneath was water. The speed of sound in water was calibrated in our laboratory

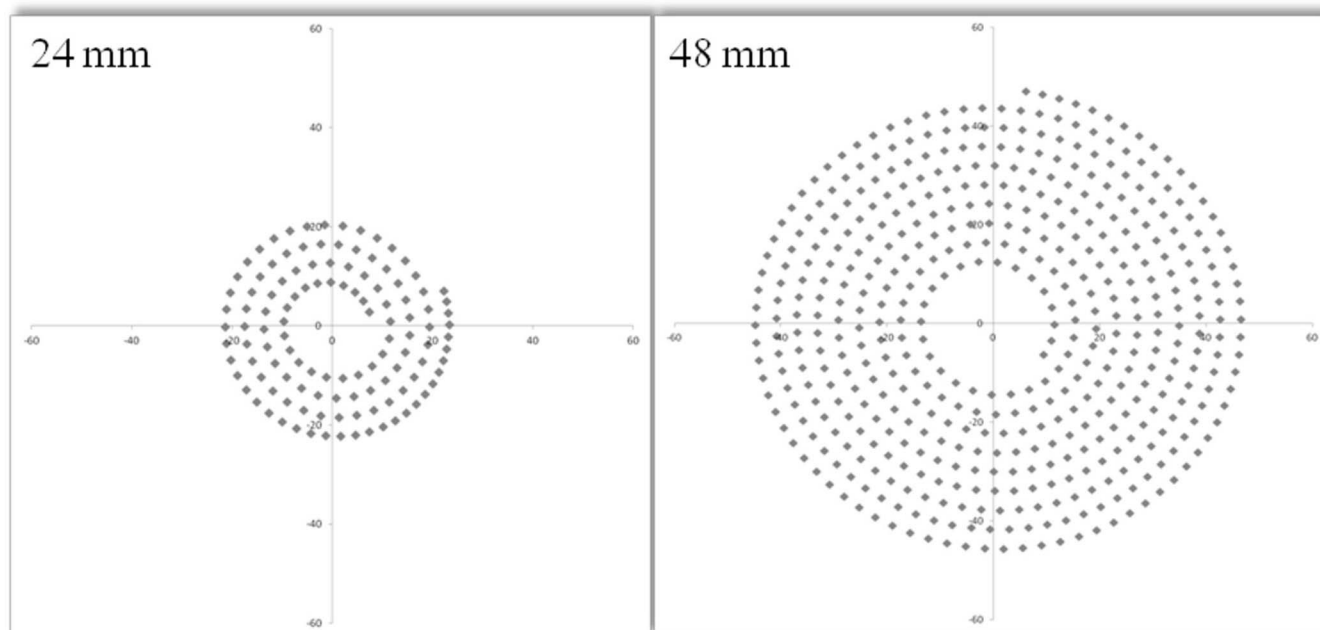


FIG. 4. Two of the spiral scan patterns used in this report: (a) our smallest spiral (120 locations, radius = 24 mm), and (b) a larger spiral (480 locations, radius = 48 mm). Note that the spacing between discrete locations is approximately the same for both spirals.

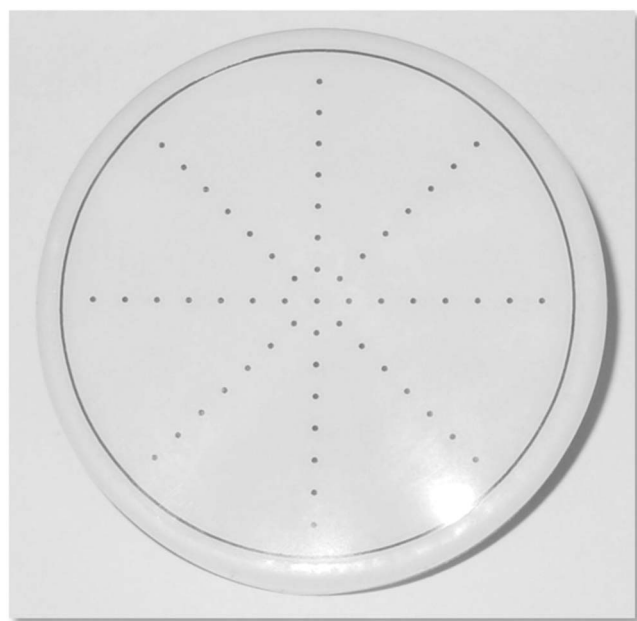


FIG. 5. A contrast phantom was fabricated by printing 1 mm red dots on a transparent film and attaching it to a 1-cm-thick disk of PVCp. The dots are spaced 5 mm apart radially and enclosed by an 80 mm diameter circle. The absorption of the red dots was equivalent to the absorption of 1 mm blood thickness at 756 nm.

as a function of temperature, which was recorded during data acquisition. We chose the sound speed within the breast phantom interactively by visually assessing the “sharpness” of vessels within the breast phantom as the assumed sound speed above the breast cup of the scanner was varied.

To quantify the contrast-to-noise performance of the PAM system, we imaged the phantom we developed as shown in Fig. 5. It consisted of an array of 1-mm “red” dots printed on a disk of clear plastic with an HP color laser printer and affixed to a 1-cm thick disk of polyvinylchloride-plastisol (PVCp) to provide rigidity. The absorbance of the red ink dot at 756 nm was measured with a *Genesys 10vis* spectrophotometer.

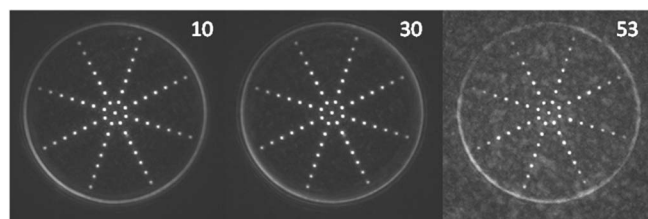


FIG. 7. PAM images (24 mm spiral scan) of the contrast phantom through 10, 30, and 53 mm of 8% LiposynII-20%. The contrasts of the three images have been normalized to one another.

ter as 0.129, which is approximately the same absorbance one expects for a 1-mm thick sample of blood containing 150 g/L of oxyhemoglobin.⁹ Therefore, based on this data, we concluded this to be reasonably equivalent to blood absorption by a 1-mm-thick blood vessel.

Next, we filled the breast cup of the scanner with an 8% solution of stock Liposyn II-20%¹⁹ to simulate the attenuation of breast tissue (attenuation coefficient = 1.1 cm^{-1}). The contrast phantom was placed at varying depths within the Liposyn solution, as shown in Fig. 6. PAM images of the phantom were acquired using a 24-mm spiral scan with an acquisition time of 12 s.

PAM images at three depths of Liposyn solution were acquired and are shown in Fig. 7. Both contrast and noise were measured from those images as a function of depth of Liposyn solution between the breast cup of the scanner and the location of the contrast phantom in the breast cup. The contrast and contrast-to-noise ratios were then recorded, plotted as a function of depth of Liposyn solution, and analyzed.

To measure spatial resolution of the PAM scanner, we imaged a long filament ($6 \mu\text{m}$ diameter) of graphite fiber embedded in an agar mold, shaped to fit snugly into the scanner breast cup. A photograph of the graphite phantom and a MIP calculated from a 3D PAM image (48-mm spiral scan, 48 s) are shown in Fig. 8. The full width at half-maximum (FWHM) of a profile across one of the carbon fibers was used to estimate the spatial resolution of the PAM system.

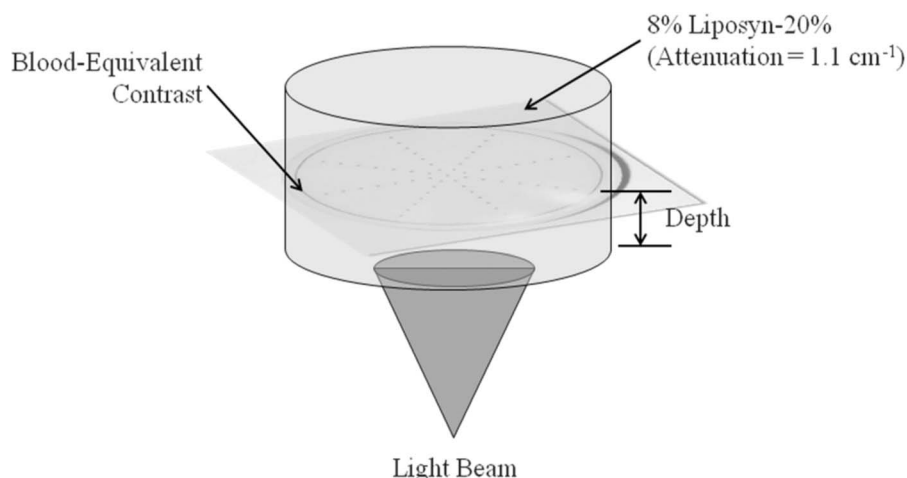


FIG. 6. Imaging geometry for measuring contrast and noise using the phantom pictured in Fig. 4 as a function of depth of breast-tissue-mimicking liquid (8% LiposynII-20%).

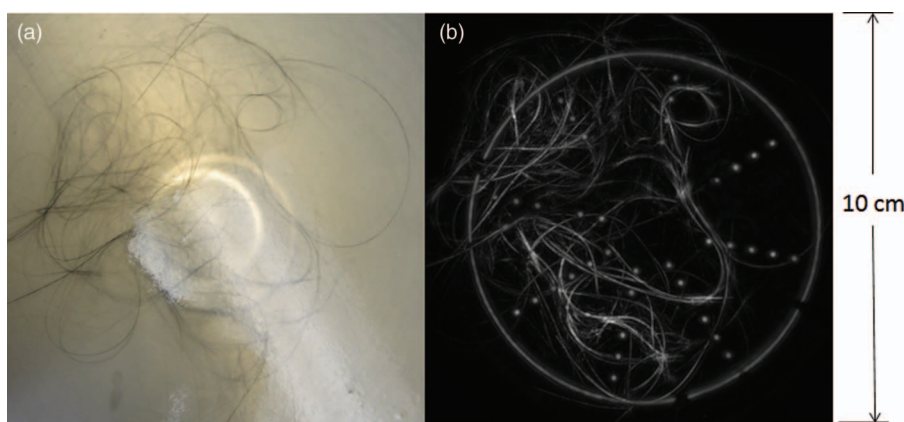


FIG. 8. (a) Photograph of carbon fiber (6 μm diameter) placed in agar mold. (b) MIP of PAM image of carbon-fiber phantom. In making the photoacoustic image, we placed the dot phantom (Figure 5) atop the agar to keep it from floating, so it is projected on the photoacoustic image of the graphite filament phantom. [Image of 1 mm dot phantom (Figure 5) provides scale.]

In order to demonstrate that we could maintain good contrast, sensitivity, and spatial resolution at the periphery of the field of view, we translated our contrast phantom laterally 80 mm and scanned with our largest spiral protocol (96 mm, 3.2 min).

Four healthy women volunteers were recruited according to a protocol approved by the Institutional Review Board of the University of North Carolina. Each of these volunteers was greater than 40 years of age and had a normal screening mammogram within the 12 months prior to PAM imaging. The breast sizes and mammographic breast densities were recorded for each volunteer. Prior to patient positioning by a trained mammography research technologist, a few hundred mL of clean water were placed in the imaging cup of the scanner and the patient was positioned prone on the exam table, placing her left breast approximately in the center of the cup of the scanner. The patient's right arm was positioned in an arc above her head and her left arm was placed along her left side (left "swim" position). Additional clean water was added to fill to the top of the cup of the scanner as needed. The patient was then instructed to lie still and breathe normally during the 3.2 min breast scan/data acquisition. A 96-mm spiral was used for data acquisition. After imaging the left breast, the right breast was positioned, as above, and imaged in an identical fashion, interchanging the positions of the left and right arm (right "swim" position).

Three-dimensional PAM images of each breast for each volunteer were reconstructed on $1024 \times 1024 \times 300$ voxels (.25 mm on a side) using filtered backprojection. To compensate for the exponential loss of PAM contrast as a function of the thickness of breast tissue, the reconstructed images were further processed by applying a depth-dependent, exponential scaling, $e^{\alpha z}$, where z is distance (cm) along the anterior-posterior (AP) axis, and α is a constant that could be adjusted retrospectively. Reconstruction took approximately 25 min using three NVIDIA K20 GPU cards. In addition, we calculated maximum-intensity projections (MIPs) in both the medial-lateral (ML) and the coronal projections for image display.

3. RESULTS

The photoacoustic contrast for the center "dot" of our contrast target (Fig. 7) was measured and plotted as a function of the depth of the 8% Liposyn II-20% solution. The result is plotted in Fig. 9(a) and displays exponential decay with

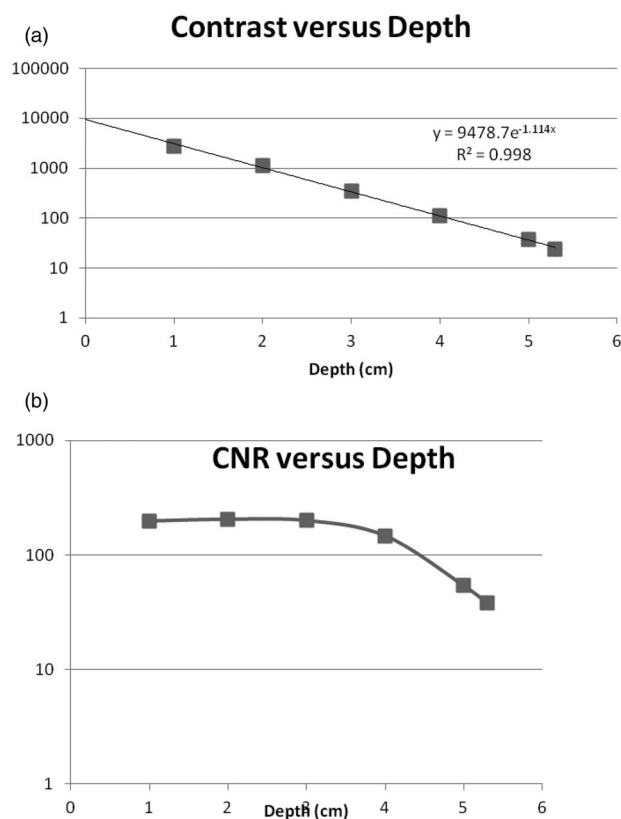


FIG. 9. (a) Contrast as a function of depth in Liposyn II solution. The data, when fit to an exponential, revealed an effective attenuation coefficient of 1.1 cm^{-1} . (b) Contrast-to-noise ratio (CNR) was calculated from images such as those displayed in Fig. 7. The CNR was approximately constant (~ 200) for depths < 30 mm and was limited by streak noise, which is proportional to contrast. For greater depths, the system electronic noise [~ 1 unit on Fig. 9(a)] began to degrade the CNR.

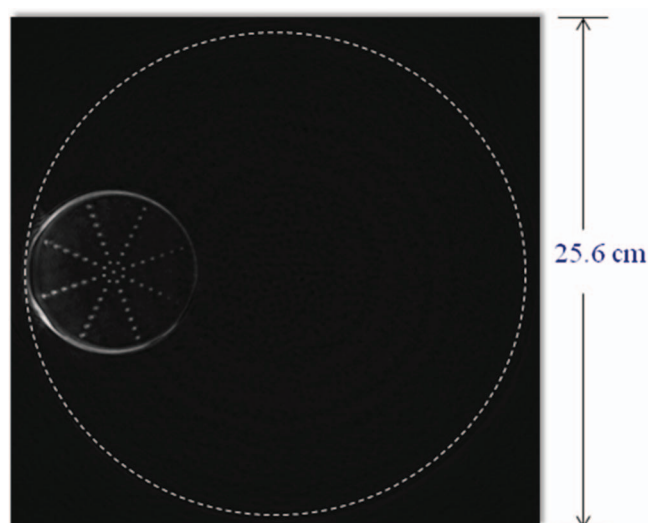


FIG. 10. PAM image of contrast phantom displaced 80 mm laterally from the center of the breast cup. To capture this image, the radius of the spiral scan was increased to 96 mm (1920 locations). The phantom was visualized clearly at the periphery of the image volume.

depth. The noise was calculated as the standard deviation within a small region of the background in the contrast target. This “noise” estimate was recorded and used to calculate the contrast-to-noise ratio (CNR), which is plotted in Fig. 9(b). We could not collect data for depths >53 mm due to the finite depth of the breast-restraining cup of the scanner.

The spatial resolution was estimated from a plot across one filament of the graphite fiber phantom [Fig. 8(b)]. The full width at half-maximum of the plot was 0.42 mm. This resolution did not vary much with orientation of the graphite filament, demonstrating nearly isotropic spatial resolution.

The lateral field of view was measured as 24 cm as indicated from the visibility of the contrast phantom placed at the edge of our field of view (Fig. 10).

Maximum intensity projections from the four healthy volunteer bilateral PAM exams are shown in Figs. 11 and 12. Vessels were clearly visualized back to the chest wall in all four volunteers with breast sizes that ranged from C to DD cups.

4. DISCUSSION

The results from this study indicate that we can use a dedicated photoacoustic imaging device to evaluate hemoglobin distributions in healthy human breast tissue. Initially, we began our research with the intent of adapting a preclinical photoacoustic tomography (PAT) scan design, initially used with animal models, to image the human breast.²⁰ However, the preclinical breast PAT scanner had a limited field of view (relative to a human breast), but high enough spatial resolution (0.2–0.3 mm) to visualize the vasculature in a small mammal. Penetration depth of 1–2 cm was sufficient for imaging mice, but insufficient for imaging the human breast. Lesser spatial resolution and greater tissue penetration is required in clinical breast imaging, where the vasculature has a range of diameters of 0.5–2.0 mm, but tissue penetration must approach 5 cm. Therefore, in our dedicated breast PAM system, we opted to trade spatial resolution for increased contrast sensitivity. This was done by reducing the center frequency of our ultrasound transducers from 5 to 2 MHz. In addition, greater optical fluence was used to increase the dynamic range of the system.

The greatest challenge, however, was to find a way to increase the field of view of the system dramatically, which was ultimately limited by the angular sensitivity of our circular transducers, without sacrificing contrast sensitivity. Choosing

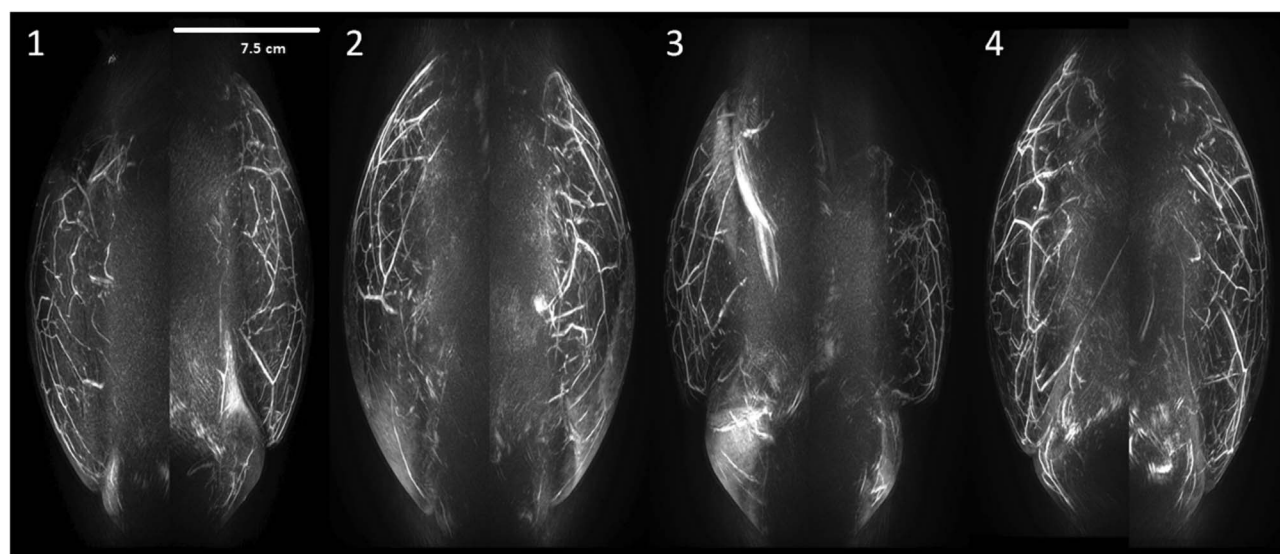


FIG. 11. Maximum intensity projections in the medial-lateral (ML) projection of bilateral PAM exams of four healthy volunteers with known mammographic breast density and brassiere cup size (back-to-back images: left breast on right, right breast on left as is normally presented clinically for x-ray mammograms): (1) heterogeneously dense, D cup; (2) scattered fibroglandular densities, DD cup; (3) scattered fibroglandular densities, C cup; and (4) scattered fibroglandular densities, DD cup. Please note that the front surface of the breasts, being pliable, assume the smooth shape of the breast cup.

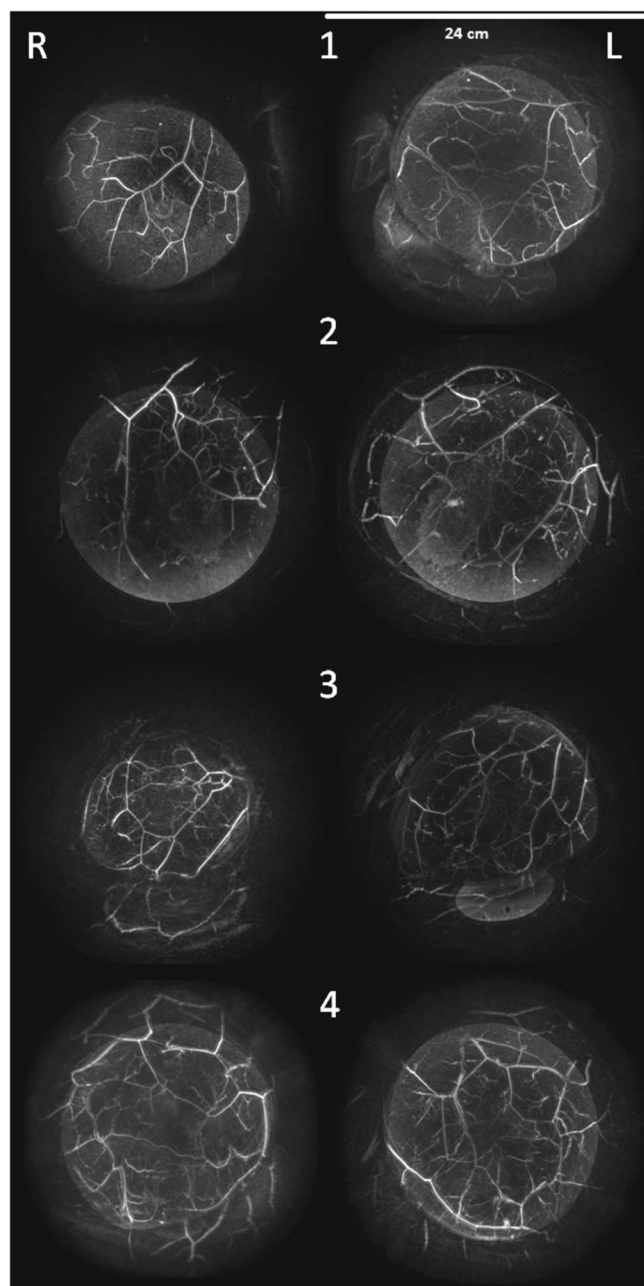


FIG. 12. Maximum intensity projections in the coronal projection of bilateral PAM exams of the four healthy volunteers.

smaller diameter transducers elements would have increased the FOV, but at the expense of contrast sensitivity, and therefore was not a viable option. Instead, we chose to change the manner of scanning the detector array to increase projection density. We chose to scan the PAM array continuously in a spiral pattern during data acquisition, rather than rotating the array about its vertical axis as had been done in our previous prototype PAT scanner. This new spiral scan protocol increased the density of projections while simultaneously increasing the FOV. By adjusting the number of projection angles in proportion to the projected *area* encompassed by the spiral scan, we were able to maintain contrast sensitivity and

spatial resolution for arbitrarily large fields of view as needed in breast imaging.

Our dedicated photoacoustic mammography (PAM) scanner now consists of a hemispherical detection aperture that is translated laterally in a spiral pattern, which permits acquisition of 3D photoacoustic images over a 24-cm lateral field of view. Using this PAM scanning system, we demonstrated sufficient contrast-to-noise to visualize a 1-mm, blood-equivalent target through at least 5.3 cm of an optical scattering medium that displayed an optical attenuation of 1.1 cm^{-1} . This optical attenuation is typical of what has been measured for breast tissue.^{10,11} We note that the CNR remained constant through the first 3.0 cm of turbid media before dropping as the depth increased. The reason for this behavior, we believe, is the result of the dominance of “streak noise,” which is proportional to photoacoustic (PA) contrast. The streak noise is much greater than the electronic noise “floor” of the input electronics of our data acquisition system at shallow depths, where PA contrast is highest. As the PAM contrast falls to lower levels at greater depths, the electronic noise begins to degrade our CNR, as we have demonstrated in Fig. 9. We estimated the spatial resolution of our PAM scanner as 0.42 mm, which is only slightly greater than the theoretical minimum of 0.38 mm ($\lambda/2$) due to the 2 MHz transducers used in our scanner.

We have improved the contrast sensitivity of our previous photoacoustic detector array by reducing the center frequency of our transducer from 5 MHz to 2 MHz as we speculated in our previous work.¹⁶ As we then noted, the peak response of our 5 MHz transducer lay outside the 4.0 MHz passband of our reconstruction filter and above the predominant, photoacoustic temporal frequencies generated by vascular structures and tumors (>0.5 mm diameter) within the breast. The peak response of our 2 MHz transducers now better overlaps these temporal frequencies.

The thickness of the breast tissue was compressed to 2.3–4.0 cm, depending on the size of the breast being imaged. The compression was the result of the patient being in the prone position on the scanning table and not the result of a compression paddle as used in conventional mammography. The bilateral breast images demonstrated good vessel visibility throughout the parenchyma of both breasts of all the volunteers. Contrast equalization ($e^{\alpha z}$, $\alpha = 1.0$) successfully compressed the dynamic range of our PAM so that all vessels could be simultaneously visualized, regardless of depth. Based on our phantom studies, we expect to be able to image through as much as 5.3 cm of tissue for larger breasts, or a breast with a volume as large as 1335 mL. This represents the 90th percentile of breast volumes encountered in clinical practice in the United States.²¹

5. CONCLUSION

We have developed a dedicated photoacoustic mammography system capable of imaging blood vessels throughout an entire human breast with submillimeter spatial resolution. Through upcoming clinical trials, we will evaluate the

feasibility of PAM in the evaluation of the vascular network present in both malignant and benign breast lesions.

ACKNOWLEDGMENTS

This work was sponsored in part by funding from the National Institutes of Health, HHS Grant No. CA160850.

^{a)} Author to whom correspondence should be addressed. Electronic mail: bobkruger@optosonics.com

- ¹ J. Fracheboud, S. J. Otto, J. A. van Dijk, M. J. Broeders, A. L. Verbeek, and H. J. de Koning, "National evaluation team for breast cancer screening (NETB): Decreased rates of advanced breast cancer due to mammography screening in the Netherlands," *Br. J. Cancer* **91**(5), 861–867 (2004).
- ² N. G. Coburn, M. A. Chung, J. Fulton, and B. Cady "Decreased breast cancer tumor size, stage, and mortality in Rhode Island: An example of a well-screened population," *Cancer Control* **11**(4), 222–230 (2004).
- ³ I. Jatoi, B. E. Chen, W. F. Anderson, and P. S. Rosenberg, "Breast cancer mortality trends in the United States according to estrogen receptor status and age at diagnosis," *J. Clin. Oncol.* **25**(13), 1683–1690 (2007).
- ⁴ A. A. Oraevsky *et al.*, "Optoacoustic imaging of blood for visualization and diagnostics of breast cancer," *Biomed. Optoacoust.* **4618**, 81–94 (2002).
- ⁵ C. G. A. Hoelen, F. F. M. de Mul, R. Pongers, and A. Dekker, "Three-dimensional photoacoustic imaging of blood vessels in tissue," *Opt. Lett.* **23**, 648–650 (1998).
- ⁶ S. R. McDougall, A. R. A. Anderson, and M. A. J. Chaplain "Mathematical modeling of dynamic adaptive tumor-induced angiogenesis: Clinical implications and therapeutic targeting strategies," *J. Theor. Biol.* **241**, 564–589 (2006).
- ⁷ J. Folkman, "Tumor angiogenesis: Therapeutic implications," *N. Engl. J. Med.* **285**, 1182–1186 (1971).
- ⁸ B. J. Tromberg *et al.*, "Assessing the future of diffuse optical imaging technologies for breast cancer management," *Med. Phys.* **35**(6), 2443–2451 (2008).
- ⁹ S. Wray *et al.*, "Characterization of the near infrared absorption spectra of cytochrome aa3 and haemoglobin for the non-invasive monitoring of cerebral oxygenation," *Biochim. Biophys. Acta* **933**(1), 184–192 (1988).
- ¹⁰ A. Pifferi *et al.*, "Spectroscopic time-resolved diffuse reflectance and transmittance measurements of the female breast at different interfiber distances," *J. Biomed. Opt.* **9**(6), 1143–1151 (2004).
- ¹¹ A. Cerussi, N. Shah, D. Hsiang, A. Durkin, J. Butler, and B. J. Tromberg, "In vivo absorption, scattering, and physiologic properties of 58 malignant breast tumors determined by broadband diffuse optical spectroscopy," *J. Biomed. Opt.* **11**(4), 044005 (2006).
- ¹² J. J. Heine and J. A. Thomas, "Effective x-ray attenuation coefficient measurements from two full field digital mammography systems for data calibration applications," *BioMedical Engineering OnLine* **7**, 13–24 (2008).
- ¹³ A. A. Oraevsky, R. O. Esenaliev, S. L. Jacques, F. K. Tittel, and D. Medina, "Breast cancer diagnostics by laser optoacoustic tomography," in *Trends in Optics and Photonics*, edited by R. R. Alfano and J. G. Fujimoto (OSA Publishing House, Washington, DC, 1996), pp. 316–321.
- ¹⁴ C. Haisch *et al.*, "Combined optoacoustic/ultrasound system for tomographic absorption measurements: Possibilities and limitations," *Anal. Bioanal. Chem.* **397**, 1503–1510 (2010).
- ¹⁵ S. Manohar, A. Kharine, J. C. G. van Hespén, W. Steenbergen, and T. G. van Leeuwen, "Photoacoustic mammography laboratory prototype: Imaging of breast tissue phantoms," *J. Biomed. Opt.* **9**, 1172–1181 (2004).
- ¹⁶ R. A. Kruger, R. B. Lam, D. R. Reinecke, S. P. DelRio, and R. P. Doyle "Photoacoustic angiography of the breast," *Med. Phys.* **37**(11), 6096–7000 (2010).
- ¹⁷ American National Standard for Safe Use of Lasers, ANSI Z136.1–2007, p. 95.
- ¹⁸ Y. Wang, Y. Zeng, and Q. Chen, "Photoacoustic imaging with deconvolution algorithm," *Phys. Med. Biol.* **49**, 3117–3124 (2004).
- ¹⁹ Liposyn II 20% is an intravenous fat emulsion containing 10% safflower oil, 10% soybean oil, 1.2% egg phosphatides, and 2.5% glycerin in water.
- ²⁰ R. A. Kruger *et al.*, "HYPR-Spectral photoacoustic CT for preclinical imaging," *Proc. SPIE* **7177**, 71770F (2009).
- ²¹ S.-Y. Huang *et al.*, "The characterization of breast anatomical metrics using dedicated breast CT," *Med. Phys.* **38**(4), 2180–2191 (2011).